A DC Stable and Large Time Step Well-Balanced TD-EFIE Based on Quasi-Helmholtz Projectors

Yves Beghein, Kristof Cools, and Francesco P. Andriulli, *Senior Member, IEEE*

***Abstract*—The marching-on-in-time solution of the time domain electric field integral equation (TD-EFIE) has traditionally suffered from a number of issues, including the emergence of spurious static currents (DC instability) and ill-conditioning at large time steps (low frequencies). In this contribution, a space-time Galerkin discretization of the TD-EFIE is proposed, which separates the loop and star components of both the equation and the unknown. Judiciously integrating or differentiating these components with respect to time leads to an equation which is free from DC instability. By choosing the correct temporal basis and testing functions for each of the components, a stable marching-on-in-time system is obtained. Furthermore, the scaling of these basis and testing functions ensure that the system remains well-conditioned for large time steps. The loop-star decomposition is performed using quasi-Helmholtz projectors in order to avoid the explicit transformation to the unstable bases of loops and stars (or trees), and to avoid the search for global loops, which is a computationally expensive operation.**

***Index Terms*—time domain, electric field integral equation, DC instability, low frequency breakdown.**

I. Introduction

ELECTROMAGNETIC scattering by perfect electrical conductors can be modeled efficiently using boundary integral equations (BIEs). The two most prominent formulations are the electric field integral equation (EFIE) and the magnetic field integral equation (MFIE). This paper focusses on the properties of the EFIE.

The EFIE can be formulated in either the frequency domain (FD-EFIE, for time-harmonic electromagnetic fields) or the time domain (TD-EFIE, for general time dependence). Whereas the FD-EFIE is solved at a single point on the frequency axis, the TD-EFIE requires a discretization of the time axis. Most often, a causal discretization scheme is chosen such that the resulting system of equations can be solved using the marching-on-in-time (MOT) algorithm [1], [2] (other approaches such as marching-on-in-order have been suggested, see e.g. [3]). The stability of the MOT algorithm hinges on both the accurate evaluation of the interaction integrals [4]–[7] and the choice of temporal discretization scheme [8]–[11]. Space-time Galerkin schemes have been found to produce good results in terms of stability, accuracy and extensibility to higher order in both space and time [10], [12]–[14].

Unfortunately, these schemes suffer from at least one of the following problems.

Y. Beghein is with the Department of Information Technology (INTEC), Ghent University, Belgium, yves.beghein@ugent.be.

K. Cools is with the Electrical Systems and Optics Research Division, University of Nottingham, Nottingham NG7 2RD, U.K.

F.P. Andriulli is with the Microwave Department of Telecom Bretagne – Institut Mines-Telecom, Brest, France.

First, the TD-EFIE allows sourceless harmonic-in-time regime solutions. When the scatterer is closed, interior resonances can be excited (resonant instabilities) [15], [16]. Furthermore, it supports sourceless constant or linear in time divergence free solutions (DC instabilities) [16], [17]. For simply connected geometries, DC instabilities can be eliminated by switching to the Calderón preconditioned TD-EFIE [18] and applying the so-called dot-trick [16]. However, for multiply connected geometries, the dot-trick EFIE still supports static solutions [19] and is therefore susceptible to DC instability.

Second, for large time steps Δt, the scaling of the blocks of the TD-EFIE operator that describe the electrostatic and and magnetostatic problems differs by a factor Δt^2, leading to an ill conditioned system matrix. The resulting system cannot be solved efficiently (using e.g. iterative techniques), which drastically increases the solution time. This phenomenon is termed low frequency breakdown [20], [21], and also occurs in the frequency domain, see e.g. [22], [23] and references therein.

Finally, the standard TD-EFIE involves the computation of the charge as the temporal integral of the current divergence at every time step. This computationally costly operation is often avoided by introducing an additional charge variable (at the cost of greater memory requirements), or by switching to the time-differentiated TD-EFIE (at the cost of introducing linear-in-time spurious loop currents to the solution).

Low frequency breakdown can be mitigated by applying a loop-star or loop-tree decomposition to the EFIE, and rescaling the components with the correct powers of Δt [21]. However, explicitly constructing a basis of loops and stars (or trees) leads to ill-conditioning [24]. Furthermore, for multiply connected surfaces, global loops must be detected, which is computationally expensive.

Linear-in-time spurious currents have also been tackled by applying a loop-tree decomposition to the time-differentiated TD-EFIE in [25]. While this does result in the elimination of the linear-in-time spurious currents, it does not solve constant-in-time DC instability. In [26], a loop-tree decomposition is used to filter out static loop modes after they emerge.

In this contribution, a novel formulation termed the quasi-Helmholtz Projected TD-EFIE (qHP-TDEFIE) is obtained by separating the quasi-Helmholtz components of both spatial basis and testing functions using the loop and star projectors introduced in AndriulliMultConn, thereby eliminating the need to explicitly construct a loop-star basis. The loop and star parts of both the equation and the unknown are temporally integrated or differentiated in such a way that the resulting equation does not possess a static nullspace, and is therefore

not susceptible to DC instability. Furthermore, it does not require the computation of the temporal integral of the current.

Next, the quasi-Helmholtz components of both the unknown and the equation are separately discretized in time using Galerkin methods. More specifically, the order of regularity of the basis and testing functions is matched to the order of differentiation of each component. This is necessary in order to obtain a stable MOT scheme. Furthermore, the scaling of the basis and testing functions is chosen such that system has a well-defined and well-conditioned low frequency limit. In addition, the interaction matrix elements needed in this scheme are compatible with matrix-vector product accelerators such as the PWTD method [27], [28].

This paper is organized as follows. In Section II, the standard TD-EFIE is presented in order to fix the notations and definitions that will be used throughout the paper. The properties of the resulting MOT algorithm are summarily reviewed. In Section III, the derivation of the new qHP-TDEFIE is presented and discussed. In Section IV, the low frequency (large time step) limit of the resulting numerical scheme is investigated. Finally, a number of numerical experiments are performed in Section V to demonstrate the favourable properties of the qHP-TDEFIE formulation, both in terms of DC stability and independence of the condition number on the time step size.

II. The Standard EFIE and Its Properties

A. The Time Domain EFIE

Consider a perfectly conducting body Ω, whose boundary is denoted Γ. When an incident electric field $\boldsymbol{e}^i(\boldsymbol{r},t)$ impinges on it at $t>0$, a surface current $\boldsymbol{j}(\boldsymbol{r},t)$ is induced on Γ, that satisfies the time domain EFIE

$$\eta\left(\mathcal{T}\boldsymbol{j}\right)(\boldsymbol{r},t) = -\hat{\boldsymbol{n}}\times\boldsymbol{e}^i(\boldsymbol{r},t) \quad \forall \boldsymbol{r}\in\Gamma, t>0, \tag{1}$$

where the electric field integral operator (EFIO) $\mathcal{T}$ is defined as

$$\begin{aligned}
\left(\mathcal{T}\boldsymbol{j}\right)(\boldsymbol{r},t) &= \mathcal{T}_s\boldsymbol{j}(\boldsymbol{r},t)+\mathcal{T}_h\boldsymbol{j}(\boldsymbol{r},t), &(2)\\
\left(\mathcal{T}_s\boldsymbol{j}\right)(\boldsymbol{r},t) &= -\frac{1}{c}\hat{\boldsymbol{n}}\times\int_\Gamma \frac{\partial_t\boldsymbol{j}(\boldsymbol{r}',\tau)}{4\pi R}ds', &(3)\\
\left(\mathcal{T}_h\boldsymbol{j}\right)(\boldsymbol{r},t) &= c\;\hat{\boldsymbol{n}}\times p.v.\int_\Gamma \mathrm{grad}\frac{\partial_t^{-1}\mathrm{div}'_\Gamma\boldsymbol{j}(\boldsymbol{r}',\tau)}{4\pi R}ds' &(4)
\end{aligned}$$

$\eta=\sqrt{\mu_0/\epsilon_0}$, $c=1/\sqrt{\epsilon_0\mu_0}$, $R=|\boldsymbol{r}-\boldsymbol{r}'|$, $\tau=t-R/c$, and $\hat{\boldsymbol{n}}$ is the exterior normal vector to Γ. Define $\partial_t^{-1}f(t)=\int_{-\infty}^t f(\tau)d\tau$.

Note that (1) in itself only defines the current $\boldsymbol{j}$ up to a constant solenoidal part. Uniqueness is achieved by imposing causality, i.e., all fields are assumed to vanish for $t<0$ in a neighborhood of Ω. Causality also guarantees that $\partial_t^{-1}f(t)=\int_{-\infty}^t f(\tau)d\tau$ is well defined.

B. Standard Galerkin Discretization

The surface Γ is now approximated by a triangle mesh with N_V vertices, N_S edges, and N_C cells. On this mesh, N_S Rao-Wilton-Glisson (RWG) functions are constructed [29]. Each

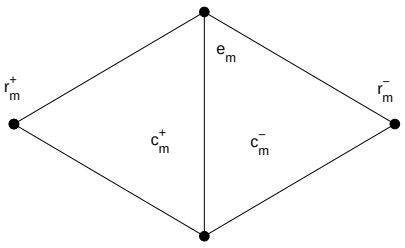

Fig. 1. Two adjacent cells on which an RWG function is defined.

RWG function $\boldsymbol{f}_m(\boldsymbol{r})$ is associated with one edge e_m (see Fig. 1), and is defined on the two adjacent cells c_m^+ and c_m^-:

$$\boldsymbol{f}_m(\boldsymbol{r}) = \begin{cases} \frac{\boldsymbol{r}-\boldsymbol{r}_m^+}{2A_{c_m^+}} & \text{for } \boldsymbol{r}\in c_m^+ \\ \frac{\boldsymbol{r}_m^- -\boldsymbol{r}}{2A_{c_m^-}} & \text{for } \boldsymbol{r}\in c_m^- \end{cases}, \tag{5}$$

where $A_{c_m^+}$ and $A_{c_m^-}$ denote the area of cell c_m^+ and c_m^-, respectively. Note that this definition does not include edge length normalization, in order to simplify the notation in what follows.

The current $\boldsymbol{j}(\boldsymbol{r},t)$ is approximated as an expansion in these RWG functions:

$$\boldsymbol{j}(\boldsymbol{r},t)=\sum_{m=1}^{N_S}\mathsf{j}_m(t)\boldsymbol{f}_m(\boldsymbol{r}). \tag{6}$$

Next, (1) is spatially tested with the rotated RWG functions $\hat{\boldsymbol{n}}\times\boldsymbol{f}_m(\boldsymbol{r})$, $m=1,2,...,N_S$:

$$\int_\Gamma \left(\hat{\boldsymbol{n}}\times\boldsymbol{f}_m(\boldsymbol{r})\right)\cdot(\text{Eq. (1)})\,ds. \tag{7}$$

By defining the following quantities:

$$\begin{aligned}
\mathcal{Z} &= \mathcal{Z}_s+\mathcal{Z}_h, &(8a)\\
\left[\left(\mathcal{Z}_s\mathsf{j}\right)(t)\right]_m &= -\sum_n\frac{\eta}{c}\int_\Gamma ds\;\boldsymbol{f}_m\cdot \\
&\qquad \int_\Gamma ds'\;\frac{\partial_t\mathsf{j}_n(\tau)\boldsymbol{f}_n(\boldsymbol{r}')}{4\pi R}, &(8b)\\
\left[\left(\mathcal{Z}_h\mathsf{j}\right)(t)\right]_m &= -\sum_n\eta c\int_\Gamma ds\;\left(\mathrm{div}_\Gamma\boldsymbol{f}_m(\boldsymbol{r})\right)\cdot \\
&\qquad \int_\Gamma ds'\;\frac{\partial_t^{-1}\mathsf{j}_n(\tau)\;\mathrm{div}'_\Gamma\boldsymbol{f}_n(\boldsymbol{r}')}{4\pi R}, &(8c)\\
\left[\mathsf{e}(t)\right]_m &= \int_\Gamma \boldsymbol{f}_m(\boldsymbol{r})\cdot\boldsymbol{e}^i(\boldsymbol{r},t)\;ds, &(8d)
\end{aligned}$$

equation (7) can be concisely stated as

$$\mathcal{Z}\mathsf{j}(t)=-\mathsf{e}(t) \qquad \forall t>0. \tag{9}$$

This equation is temporally discretized using a Galerkin method (alternatively, a collocation method can also be used – see Appendix A). The RWG expansion coefficients $\mathsf{j}_m(t)$ are approximated by an expansion in pulse functions $p(t-i\Delta t)$ (Fig. 2, middle)

$$\mathsf{j}(t)=\sum_{i=1}^{N_T}\mathsf{j}_i p(t-i\Delta t), \tag{10}$$

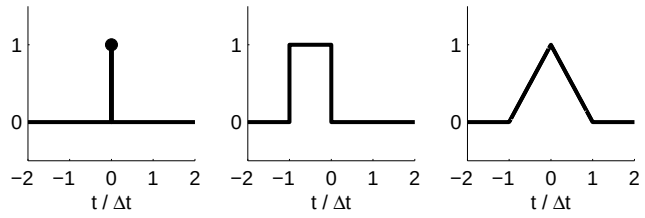

Fig. 2. Temporal basis and testing functions: Dirac delta distrubtion $\delta(t)$ (left), pulse $p(t)$ (middle) and hat $h(t)$ (right).

$$p(t) = \begin{cases} 1 & t \in (-\Delta t, 0) \\ 0 & \text{otherwise} \end{cases}, \tag{11}$$

and (9) is tested with pulses $p(t - j\Delta t)$:

$$\int_{\mathbb{R}} p(t - j\Delta t)\,(\text{Eq. (9)})\,dt \qquad j = 1, 2, 3, ..., N_T. \tag{12}$$

This can be written as

$$\sum_{i=0}^{j} \mathsf{Z}_i \mathsf{j}_{j-i} = -\mathsf{e}_j \qquad j = 1, 2, 3, ..., N_T, \tag{13}$$

where

$$\mathsf{e}_j = \int_{\mathbb{R}} p(t - j\Delta t)\ \mathsf{e}(t) dt, \tag{14}$$

$$\begin{aligned} & [\mathsf{Z}_i]_{mn} \\ = \ & \eta \int_{\mathbb{R}} dt\ p(t - i\Delta t) \int_{\Gamma} (\hat{\boldsymbol{n}} \times \boldsymbol{f}_m(\boldsymbol{r})) \cdot \mathcal{T}\left\{\boldsymbol{f}_n p\right\}(\boldsymbol{r}, t) ds \\ = \ & \Delta t \int_{\Gamma} (\hat{\boldsymbol{n}} \times \boldsymbol{f}_m(\boldsymbol{r})) \cdot \mathcal{T}\left\{\boldsymbol{f}_n h\right\}(\boldsymbol{r}, i\Delta t) ds, \end{aligned} \tag{15}$$

where $h(t)$ denotes the hat function (Fig. 2, right):

$$h(t) = \begin{cases} 1 + \frac{t}{\Delta t} & t \in (-\Delta t, 0) \\ 1 - \frac{t}{\Delta t} & t \in (0, \Delta t) \\ 0 & \text{otherwise} \end{cases}. \tag{16}$$

In (15), the interaction elements are transformed into the form encountered in traditional collocation-in-time methods. These integrals can be evaluated using techniques outlined in e.g. [4]–[7]. It is also possible to accelerate these computations using fast techniques such as PWTD [27], [28]. The system of linear equations (13) can be solved by recasting it in the following form

$$-\mathsf{Z}_0 \mathsf{j}_i = \sum_{j=1}^{i} \mathsf{Z}_j \mathsf{j}_{i-j} + \mathsf{e}_i, \tag{17}$$

which is then successively solved for j_i, $i = 1, 2, ..., N_T$. This is the marching-on-in-time (MOT) method.

Because of the temporal integral in the hypersingular contribution, there are an unlimited number of matrices $\mathsf{Z}_i \neq 0$. The number of nonzero terms in the summation in the right hand side therefore grows without bound when the MOT algorithm progresses. The unbounded summation can be avoided by introducing the charge as an additional variable, see e.g. [11] or [30]. This however leads to overhead in both memory requirements and computation time.

C. Null Space of the Discretized EFIO

In Section II-A, it was noted that the sourceless EFIE supports constant solenoidal regime solutions. This property is conserved by the discretization procedure: if j_L is a solenoidal current,

$$\sum_{j=0}^{\infty} \mathsf{Z}_j \mathsf{j}_L = 0. \tag{18}$$

In the continuous case, an energy argument shows that late time constant signals cannot be part of the solution. Indeed, all energy in the incident wave is reflected during scattering, leaving no energy to sustain a residual magnetostatic field. In the discrete case, the finite precision of the numerical scheme allows static loop currents to creep into the solution, after which they persist throughout the simulation [17].

Even though the solution to the discrete EFIE will always be an approximation of the exact solution, it is possible to design a scheme that explicitly coerces late time energy conservation and thus cannot support DC signals in the tail of the approximate solution. In practice this property can be checked by inspecting the expressions for the interaction elements and keeping track of the explicit appearance of divergence and differentation operators. In the next section, the EFIE is rewritten and discretised in such a way that the resulting discrete system does not sustain constant-in-time regime solutions.

III. The quasi-Helmholtz Projected TD-EFIE

A. Separation of the Quasi-Helmholtz Components

In [22], the quasi-Helmholtz components (i.e., the divergence free and weakly curl free components) of the FD-EFIE are separated not by explicitly constructing a loop-star basis, but using projection matrices $\mathsf{P}^{\Lambda H}$ and P^{Σ}.

Consider a triangle mesh consisting of N_C cells, on which N_S RWG functions $\boldsymbol{f}_m(\boldsymbol{r})$ are defined. Each RWG function $\boldsymbol{f}_m(\boldsymbol{r})$ is defined on two cells, c_m^+ and c_m^- (see Fig. 1), and represents a current flowing from c_m^+ to c_m^-. The $N_S \times N_C$ star coefficient matrix is given by

$$\Sigma_{ij} = \begin{cases} 1 & \text{if cell } j \text{ equals } c_i^+ \\ -1 & \text{if cell } j \text{ equals } c_i^- \\ 0 & \text{otherwise} \end{cases}. \tag{19}$$

Note that Σ^T is the discrete divergence operator in a basis of RWG functions for the current, and cellwise constant functions for the charge. Projection onto the star space is then achieved using the projection operator

$$\mathsf{P}^{\Sigma} = \Sigma \left(\Sigma^T \Sigma\right)^+ \Sigma^T, \tag{20}$$

where $\left(\Sigma^T \Sigma\right)^+$ denotes the pseudoinverse of $\Sigma^T \Sigma$. A pseudoinverse is required because the constant vector is in the kernel of Σ. Computing this pseudoinverse using standard techniques would require $\mathcal{O}(N_c^3)$ operations. Section V of [22], however, explains how this computation can be done in linear time using techniques developed in [31]. As a result, for any $N_S \times 1$ vector c, the matrix-vector product $\mathsf{P}^{\Sigma}\mathsf{c}$ can be computed in $\mathcal{O}(N_S)$ operations.

The operator $\mathbf{P}^{\Lambda H}$ projects onto the space of divergence free expansion coefficients: $\Sigma^T \mathbf{P}^{\Lambda H} = 0$. Therefore, $\mathbf{P}^{\Sigma}\mathbf{P}^{\Lambda H} = \mathbf{P}^{\Lambda H}\mathbf{P}^{\Sigma} = 0$. This also means that the loop-star decomposition is coefficient-wise orthogonal. $\mathbf{P}^{\Lambda H}$ can easily be found as

$$\mathbf{P}^{\Lambda H} = 1 - \mathbf{P}^{\Sigma}. \tag{21}$$

In this way, the detection of global loops is avoided.

B. Elimination of the Static Null Space

The quasi-Helmholtz projectors $\mathbf{P}^{\Lambda H}$ and $\mathbf{P}^{\Sigma}$ are now applied to both the test and trial side of the semi-discrete TD-EFIE (9):

$$\begin{pmatrix}\mathbf{P}^{\Lambda H} & \mathbf{P}^{\Sigma}\end{pmatrix}\begin{pmatrix}\mathcal{Z}_s & \mathcal{Z}_s \\ \mathcal{Z}_s & \mathcal{Z}_s + \mathcal{Z}_h\end{pmatrix}\begin{pmatrix}\mathbf{P}^{\Lambda H} \\ \mathbf{P}^{\Sigma}\end{pmatrix}\mathsf{j}(t) = -\mathsf{e}(t), \tag{22}$$

where $\mathcal{Z}_h\mathbf{P}^{\Lambda H} = \mathbf{P}^{\Lambda H}\mathcal{Z}_h = 0$ has been used. The operator $\mathcal{Z}_h$ (Equation (8c)) requires the evaluation of a temporal integral. This is avoided by introducing an auxiliary unknown $\mathsf{y}(t)$:

$$\begin{aligned}&\mathsf{y}(t) = \left(\partial_t^{-1}\mathbf{P}^{\Sigma} + \mathbf{P}^{\Lambda H}\right)\mathsf{j}(t) \\ \iff\quad &\mathsf{j}(t) = \left(\partial_t\mathbf{P}^{\Sigma} + \mathbf{P}^{\Lambda H}\right)\mathsf{y}(t),\end{aligned} \tag{23}$$

satisfying

$$\begin{pmatrix}\mathbf{P}^{\Lambda H} & \mathbf{P}^{\Sigma}\end{pmatrix}\begin{pmatrix}\mathcal{Z}_s & \partial_t\mathcal{Z}_s \\ \mathcal{Z}_s & \partial_t\mathcal{Z}_s + \partial_t\mathcal{Z}_h\end{pmatrix}\begin{pmatrix}\mathbf{P}^{\Lambda H} \\ \mathbf{P}^{\Sigma}\end{pmatrix}\mathsf{y}(t) = -\mathsf{e}(t). \tag{24}$$

The operator $\mathcal{Z}_s$ involves a temporal differentiation, which annihilates constant-in-time currents. Therefore, constant loop currents reside in the null space of the operator on the left hand side of (24). This is resolved by temporally integrating the loop part of (24):

$$\mathcal{Z}'\mathsf{y}(t) = -\left(\partial_t^{-1}\mathbf{P}^{\Lambda H} + \mathbf{P}^{\Sigma}\right)\mathsf{e}(t), \tag{25}$$

$$\begin{aligned}\mathcal{Z}' &= \begin{pmatrix}\mathbf{P}^{\Lambda H} & \mathbf{P}^{\Sigma}\end{pmatrix}\begin{pmatrix}\partial_t^{-1}\mathcal{Z}_s & \mathcal{Z}_s \\ \mathcal{Z}_s & \partial_t\mathcal{Z}_s + \partial_t\mathcal{Z}_h\end{pmatrix}\begin{pmatrix}\mathbf{P}^{\Lambda H} \\ \mathbf{P}^{\Sigma}\end{pmatrix} &(26)\\ &= \left(\partial_t^{-1}\mathbf{P}^{\Lambda H} + \mathbf{P}^{\Sigma}\right)\mathcal{Z}\left(\mathbf{P}^{\Lambda H} + \partial_t\mathbf{P}^{\Sigma}\right). &(27)\end{aligned}$$

Equation (25) is the quasi-Helmholtz projected TD-EFIE or qHP-TDEFIE. Note, however, that it is still continuous in time. A suitable discretization strategy is developed in the next section.

The operator $\mathcal{Z}'$ is constructed in such way that it does not require the evaluation of a temporal integral, and it does not annihilate static loop currents. It is, in essence, the inverse Fourier transform of the modified EFIE operator proposed in [22], up to irrelevant sign conventions. An alternative method to obtain this operator is explored in Appendix A.

For slowly varying fields, the off-diagonal components as well as $\partial_t\mathcal{Z}_s$ in the lower right block of (26) become negligible. The remaining dominant contributions ($\partial_t^{-1}\mathcal{Z}_s$ and $\partial_t\mathcal{Z}_h$) do neither contain explicit temporal differentiations or integrations. These diagonal terms have a physical meaning: $\partial_t^{-1}\mathcal{Z}_s$ represents the electromagnetic vector potential, and $\partial_t\mathcal{Z}_h$ the electromagnetic scalar potential.

C. Temporal Discretization

Next, the qHP-TDEFIE (25) is discretized in time. In Section II, $\mathsf{j}(t)$ was expanded in pulses. This implies that

$$\begin{aligned}&\mathsf{y}(t) &(28)\\ =\ &\left(\partial_t^{-1}\mathbf{P}^{\Sigma} + \mathbf{P}^{\Lambda H}\right)\mathsf{j}(t) &(29)\\ =\ &\sum_{i=1}^{N_T}\left(p(t-i\Delta t)\mathbf{P}^{\Lambda H} + \partial_t^{-1}p(t-i\Delta t)\mathbf{P}^{\Sigma}\right)\mathsf{j}_i. &(30)\end{aligned}$$

The testing coefficients are transformed in a similar way.

$$\begin{aligned}\mathsf{t}_i &= \int_{\mathbb{R}} p(t-i\Delta t)\mathcal{Z}\mathsf{j}(t)\ dt &(31)\\ &= \int_{\mathbb{R}} p(t-i\Delta t)\left(\partial_t\mathbf{P}^{\Lambda H} + \mathbf{P}^{\Sigma}\right)\mathcal{Z}'\mathsf{y}(t)dt &(32)\\ &= \int_{\mathbb{R}}\left(-\partial_t p(t-i\Delta t)\mathbf{P}^{\Lambda H}\right)\mathcal{Z}'\mathsf{y}(t)dt \\ &\quad + \int_{\mathbb{R}}\left(p(t-i\Delta t)\mathbf{P}^{\Sigma}\right)\mathcal{Z}'\mathsf{y}(t)dt. &(33)\end{aligned}$$

Applying this discretization scheme to the qHP-TDEFIE would, however, result in the same system as in Section II. In particular, the resulting MOT algorithm would also suffer from DC instability. This is due to the testing functions $-\partial_t p(t-i\Delta t) = \delta\left(t-(i-1)\Delta t\right) - \delta\left(t-i\Delta t\right)$, which act as discrete derivatives. Furthermore, the number of nonzero $\mathbf{Z}$-matrices would be infinite due to the infinite support of the expansion function $\partial_t^{-1}p(t-i\Delta t)$. Finally also the scaling of the two blocks remains unchanged and leads to a condition number that scales like Δt^2 at large time steps (see Section IV).

All these issues can be solved by directly discretizing (25) rather than inheriting the discretisation of the classic TD-EFIE (9). More specifically:

$$\begin{aligned}\mathsf{y}(t) &= \sum_{i=1}^{N_T}\left(p(t-i\Delta t)\mathbf{P}^{\Lambda H} + h(t-i\Delta t)\mathbf{P}^{\Sigma}\right)\mathsf{y}_i, &(34)\\ \mathsf{y}_i &= \Delta t\sum_{j=1}^{i}\mathbf{P}^{\Sigma}\mathsf{j}_j + \mathbf{P}^{\Lambda H}\mathsf{j}_i, &(35)\\ \mathsf{r}_i &= \int_{\mathbb{R}}\left(\delta(t-i\Delta t)\mathbf{P}^{\Lambda H} + \frac{1}{\Delta t}p(t-i\Delta t)\mathbf{P}^{\Sigma}\right)\mathcal{Z}'\mathsf{y}(t)dt \\ &= \frac{1}{\Delta t}\mathbf{P}^{\Sigma}\mathsf{t}_i - \sum_{j=1}^{i}\mathbf{P}^{\Lambda H}\mathsf{t}_j. &(36)\end{aligned}$$

In this discretization scheme, the loop part and the star part of $\mathsf{y}(t)$ are expanded in pulse functions $p(t-i\Delta t)$ (Fig. 2, middle) and hat functions $h(t-i\Delta t)$ (Fig. 2, right), respectively. The loop part and the star part of $\mathcal{Z}'$ are tested with Dirac delta distributions $\delta(t-i\Delta t)$ (Fig. 2, left) and pulses, respectively. Note that the basis functions of both Helmholtz components can represent the constant-in-time function and that the testing functions of neither of the Helmholtz components disappears when applied to constant-in-time functions. The basis functions of both Helmholtz components of $\mathsf{y}(t)$ are normalized to 1. The testing functions of both Helmholtz components are also scaled equally in the sense that both $\int_{\mathbb{R}}\delta(t)dt$ and

$\int_{\mathbb{R}} \frac{1}{\Delta t} p(t) dt$ equal 1. This is the origin of the factor $\frac{1}{\Delta t}$ in (36). The global factor Δt in (35) is not necessary for balancing, but results in a well defined limit for the system matrices as large time step, as will be detailed in Section IV.

This expansion and testing scheme is now applied to the qHP-TDEFIE (25).

$$\int_{\mathbb{R}} \left(\delta(t - j\Delta t) \mathbf{P}^{\Lambda H} + \frac{1}{\Delta t} p(t - j\Delta t) \mathbf{P}^{\Sigma} \right) (\text{Eq. (25)}) \; dt, \tag{37}$$

for $j = 1, 2, ..., N_T$, or

$$-\mathbf{Z}'_0 \mathsf{y}_j = \sum_{i=1}^{j} \mathbf{Z}'_i \mathsf{y}_{j-i} + \mathsf{e}'_j, \tag{38}$$

where the matrices $\mathbf{Z}'_i$ are constructed from four components

$$\mathbf{Z}'_i = \begin{pmatrix} \mathbf{P}^{\Lambda H} & \mathbf{P}^{\Sigma} \end{pmatrix} \begin{pmatrix} \mathbf{Z}'^{LL}_i & \mathbf{Z}'^{LS}_i \\ \mathbf{Z}'^{SL}_i & \mathbf{Z}'^{SS}_i \end{pmatrix} \begin{pmatrix} \mathbf{P}^{\Lambda H} \\ \mathbf{P}^{\Sigma} \end{pmatrix}, \tag{39}$$

which are explicitly given in Equations (40a)-(40d). The excitation vector e'_j is given by

$$\mathsf{e}'_j = \int_{\mathbb{R}} \left(\delta(t - j\Delta t) \partial_t^{-1} \mathbf{P}^{\Lambda H} + \frac{1}{\Delta t} p(t - j\Delta t) \mathbf{P}^{\Sigma} \right) \mathsf{e}(t) \; dt. \tag{41}$$

Once the expansion coefficients y_i are found, the physical current $\boldsymbol{j}(\boldsymbol{r}, t)$ on Γ can be computed as

$$\boldsymbol{j}(\boldsymbol{r}, t) = \sum_{m=1}^{N_S} \sum_{i=1}^{N_T} [\mathsf{j}_i]_m \; p(t - j\Delta t) \boldsymbol{f}_m(\boldsymbol{r}), \tag{42}$$

$$\mathsf{j}_i = \mathbf{P}^{\Lambda H} \mathsf{y}_i + \mathbf{P}^{\Sigma} \frac{1}{\Delta t} (\mathsf{y}_i - \mathsf{y}_{i-1}). \tag{43}$$

The use of different temporal basis and testing functions for the loop and star components is necessary to obtain a stable MOT scheme. If $y(t)$ is expanded in a single set of basis functions ($h(t - i\Delta t)$ or $p(t - i\Delta t)$), and (25) is tested with a single set of testing functions ($p(t - i\Delta t)$ or $\delta(t - i\Delta t)$), high frequency instabilities are encountered. When a stability analysis is conducted as in [16], the eigenvalues of the companion matrix are not confined to the unit circle, indicating that the scheme is unstable.

In contrast to $\mathcal{Z}$, $\mathcal{Z}'$ does not contain a temporal integral. As a consequence, the number of nonzero matrices $\mathbf{Z}'_i$ is finite in this scheme. No further manipulation or auxiliary quantities are required.

The integrals (40a)-(40d) can be interpreted as the interactions which are also found in traditional collocation-in-time schemes, meaning that they can be accelerated using fast techniques such as PWTD [27], [28].

D. Static Null Space

Consider a constant solenoidal current $\boldsymbol{j}(\boldsymbol{r}, t) = \boldsymbol{j}_L(\boldsymbol{r})$, $\text{div}_\Gamma \boldsymbol{j}(\boldsymbol{r}) = 0$, with RWG expansion coefficients $\mathsf{j}_i = \mathsf{j}_L = \mathbf{P}^{\Lambda H} \mathsf{j}_L$. This current is annihilated by the TD-EFIE operator, in the continuous as well as in the discrete setting:

$$(\mathcal{T} \boldsymbol{j})(\boldsymbol{r}, t) = 0 \quad \forall t > 0, \forall \boldsymbol{r} \in \Gamma, \tag{44}$$

$$(\mathcal{Z} \mathsf{j})(t) = 0 \quad \forall t > 0, \tag{45}$$

$$\sum_{j=0}^{i} \mathbf{Z}_j \mathsf{j}_{i-j} = 0 \quad i = 0, 1, 2, ... \tag{46}$$

This is the origin of the DC instability encountered in standard TD-EFIE simulations.

For solenoidal currents, $\mathsf{j}(t) = \mathsf{y}(t)$ and $\mathsf{j}_i = \mathsf{y}_i$. These functions are not annihilated by the qHP-TDEFIE operator:

$$(\mathcal{Z}' \mathsf{y})(t) \neq 0 \quad \forall t > 0. \tag{47}$$

Moreover, because the trial functions can resolve constant-in-time functions, this property is conserved upon temporal discretization. Therefore, the qHP-TDEFIE does not allow constant in time solenoidal currents as sourceless regime solutions. This immediately implies that the qHP-TDEFIE is not susceptible to DC instabilities.

IV. Low Frequency Limit

In this section, the low frequency limit of the system matrix $\mathbf{Z}_0$ (standard TD-EFIE, Section II) and $\mathbf{Z}'_0$ (qHP-TDEFIE, Section III) is investigated. For this, the scatterer is assumed to be small, i.e., with diameter $D \ll c\Delta t$.

A. Low Frequency Limit of the Standard TD-EFIE

The TD-EFIE system matrix is split into a singular and a hypersingular part

$$\mathbf{Z}_0 = \mathbf{Z}_0^s + \mathbf{Z}_0^h, \tag{48}$$

$$[\mathbf{Z}_0^s]_{mn} = \eta \int_{\mathbb{R}} dt \; p(t) \int_\Gamma (\hat{\boldsymbol{n}} \times \boldsymbol{f}_m(\boldsymbol{r})) \cdot \mathcal{T}_s \{\boldsymbol{f}_n p\} (\boldsymbol{r}, t) ds$$
$$= \eta \; \Delta t \int_\Gamma (\hat{\boldsymbol{n}} \times \boldsymbol{f}_m(\boldsymbol{r})) \cdot \mathcal{T}_s \{\boldsymbol{f}_n h\} (\boldsymbol{r}, 0) ds, \tag{49}$$

$$\left[\mathbf{Z}_0^h\right]_{mn} = \eta \int_{\mathbb{R}} dt \; p(t) \int_\Gamma (\hat{\boldsymbol{n}} \times \boldsymbol{f}_m(\boldsymbol{r})) \cdot \mathcal{T}_h \{\boldsymbol{f}_n p\} (\boldsymbol{r}, t) ds$$
$$= \eta \; \Delta t \int_\Gamma (\hat{\boldsymbol{n}} \times \boldsymbol{f}_m(\boldsymbol{r})) \cdot \mathcal{T}_h \{\boldsymbol{f}_n h\} (\boldsymbol{r}, 0) ds. \tag{50}$$

Here we used the fact that a temporal Galerkin scheme is equivalent with a collocation scheme with as effective basis function the anti-convolution of the basis and testing function of the Galerkin scheme (see (15)). Assuming that $D \ll c\Delta t$, the integrand of (49) is constant in time:

$$\partial_t h(0 - R/c) = \frac{1}{\Delta t} \quad \text{for} \quad R < c\Delta t \tag{51}$$

Therefore,

$$[\mathbf{Z}_0^s]_{mn} = -\mu \; \Delta t \int_\Gamma ds \boldsymbol{f}_m(\boldsymbol{r}) \cdot \int_\Gamma ds' \frac{\boldsymbol{f}_n(\boldsymbol{r}') \partial_t h(-R/c)}{4\pi R}$$
$$= -\mu \int_\Gamma ds \; \boldsymbol{f}_m(\boldsymbol{r}) \cdot \int_\Gamma ds' \; \frac{\boldsymbol{f}_n(\boldsymbol{r}')}{4\pi R}$$
$$= [\mathbf{Z}^s_{\text{stat}}]_{mn} \tag{52}$$

where $\mathbf{Z}^s_{\text{stat}}$ is the RWG discretization of the static vector potential, which is independent of Δt. For the hypersingular part, the time dependence of the integrand of (50) can be approximated by a Taylor series:

$$\partial_t^{-1} h(0 - R/c) = \Delta t \left(\frac{1}{2} + \mathcal{O}\left(\frac{R}{c\Delta t} \right) \right), \tag{53}$$

$$\begin{aligned}
\left[\mathbf{Z}_i'^{SS}\right]_{mn} &= \frac{\eta}{\Delta t}\int_{\mathbb{R}} dt\ p(t-i\Delta t)\int_\Gamma ds\ \ (\hat{\boldsymbol{n}}\times\boldsymbol{f}_m(\boldsymbol{r}))\cdot\partial_t\mathcal{T}\left\{\boldsymbol{f}_n h\right\}(\boldsymbol{r},t)\\
&= \eta\int_\Gamma ds\ \ (\hat{\boldsymbol{n}}\times\boldsymbol{f}_m(\boldsymbol{r}))\cdot\partial_t\mathcal{T}\left\{\boldsymbol{f}_n T_{ph}\right\}(\boldsymbol{r},i\Delta t), \qquad (40a)\\
\left[\mathbf{Z}_i'^{SL}\right]_{mn} &= \frac{\eta}{\Delta t}\int_{\mathbb{R}} dt\ p(t-i\Delta t)\int_\Gamma ds\ \ (\hat{\boldsymbol{n}}\times\boldsymbol{f}_m(\boldsymbol{r})()\cdot\mathcal{T}_s\left\{\boldsymbol{f}_n p\right\}(\boldsymbol{r},t)\\
&= \eta\int_\Gamma ds\ \ (\hat{\boldsymbol{n}}\times\boldsymbol{f}_m(\boldsymbol{r}))\cdot\mathcal{T}_s\left\{\boldsymbol{f}_n h\right\}(\boldsymbol{r},i\Delta t), \qquad (40b)\\
\left[\mathbf{Z}_i'^{LS}\right]_{mn} &= \eta\int_{\mathbb{R}} dt\ \delta(t-i\Delta t)\int_\Gamma ds\ \ (\hat{\boldsymbol{n}}\times\boldsymbol{f}_m(\boldsymbol{r}))\cdot\mathcal{T}_s\left\{\boldsymbol{f}_n h\right\}(\boldsymbol{r},t)\\
&= \eta\int_\Gamma ds\ \ (\hat{\boldsymbol{n}}\times\boldsymbol{f}_m(\boldsymbol{r}))\cdot\mathcal{T}_s\left\{\boldsymbol{f}_n h\right\}(\boldsymbol{r},i\Delta t), \qquad (40c)\\
\left[\mathbf{Z}_i'^{LL}\right]_{mn} &= \eta\int_{\mathbb{R}} dt\ \delta(t-i\Delta t)\int_\Gamma ds\ \ (\hat{\boldsymbol{n}}\times\boldsymbol{f}_m(\boldsymbol{r}))\cdot\partial_t^{-1}\mathcal{T}_s\left\{\boldsymbol{f}_n p\right\}(\boldsymbol{r},t)\\
&= \eta\int_\Gamma ds\ \ (\hat{\boldsymbol{n}}\times\boldsymbol{f}_m(\boldsymbol{r}))\cdot\partial_t^{-1}\mathcal{T}_s\left\{\boldsymbol{f}_n p\right\}(\boldsymbol{r},i\Delta t), \qquad (40d)\\
T_{ph}(t) &= \frac{1}{\Delta t}\int_{\mathbb{R}} p(\tau)h(t+\tau)d\tau. \qquad (40e)
\end{aligned}$$

---

leading to

$$\begin{aligned}
\left[\mathbf{Z}_0^h\right]_{mn} &= -\frac{\Delta t}{\epsilon}\int_\Gamma ds\ \mathrm{div}_\Gamma\boldsymbol{f}_m(\boldsymbol{r})\\
&\qquad p.v.\int_\Gamma ds'\frac{\mathrm{div}'_\Gamma\boldsymbol{f}_n(\boldsymbol{r}')\partial_t^{-1}h(-R/c)}{4\pi R}\\
&= \Delta t^2\left(\frac{1}{2}\left[\mathbf{Z}_{\text{stat}}^h\right]_{mn}+\mathcal{O}\left(\frac{D}{c\Delta t}\right)\right), \qquad (54)\\
\left[\mathbf{Z}_{\text{stat}}^h\right]_{mn} &= -\frac{1}{\epsilon}\int_\Gamma ds\ \nabla\cdot\boldsymbol{f}_m(\boldsymbol{r})\int_\Gamma ds'\ \frac{\nabla'\cdot\boldsymbol{f}_n(\boldsymbol{r}')}{4\pi R} \qquad (55)
\end{aligned}$$

where $\mathbf{Z}_{\text{stat}}^h$ is the RWG discretization of the static scalar potential, which is also independent of Δt.

Thus, for $c\Delta t \to +\infty$, and considering that $\mathbf{Z}_0^h = \mathbf{P}^\Sigma\mathbf{Z}_0^h\mathbf{P}^\Sigma$,

$$\begin{aligned}
\mathbf{Z}_0 \ \to\ & \mathbf{Z}_{\text{stat}}^s+\mathcal{O}\left(\frac{D}{c\Delta t}\right)\\
&+\Delta t^2\mathbf{P}^\Sigma\left(\frac{1}{2}\mathbf{Z}_{\text{stat}}^h+\mathcal{O}\left(\frac{D}{c\Delta t}\right)\right)\mathbf{P}^\Sigma, \qquad (56)
\end{aligned}$$

or

$$\mathbf{Z}_0 \to \begin{pmatrix}\mathbf{P}^{\Lambda H} & \mathbf{P}^\Sigma\end{pmatrix}\begin{pmatrix}\mathcal{O}(1) & \mathcal{O}(1)\\ \mathcal{O}(1) & \mathcal{O}(\Delta t^2)\end{pmatrix}\begin{pmatrix}\mathbf{P}^{\Lambda H}\\ \mathbf{P}^\Sigma\end{pmatrix}, \qquad (57)$$

which leads to a condition number that grows $\propto \Delta t^2$. In [21], this ill-conditioning is resolved for simply connected structures by scaling the spatial local loop functions proportionally to Δt.

B. Low Frequency Limit of the qHP-TDEFIE

The same approach is applied to the four components of the qHP-TDEFIE. First, the loop-loop-part (40d) :

$$\begin{aligned}
&\left[\mathbf{Z}_0'^{LL}\right]_{mn}\\
&= \eta\int_\Gamma ds\ \ (\hat{\boldsymbol{n}}\times\boldsymbol{f}_m(\boldsymbol{r}))\cdot\partial_t^{-1}\mathcal{T}_s\left\{\boldsymbol{f}_n p\right\}(\boldsymbol{r},0)\\
&= -\mu\int_\Gamma ds\ \boldsymbol{f}_m(\boldsymbol{r})\cdot\int_\Gamma ds'\ \frac{\boldsymbol{f}_n(\boldsymbol{r}')\ p(0-R/c)}{4\pi R} \qquad (58)
\end{aligned}$$

Since the scatterer has diameter $D < c\Delta t$,

$$\begin{aligned}
\left[\mathbf{Z}_0'^{LL}\right]_{mn} &= -\mu\int_\Gamma ds\ \boldsymbol{f}_m(\boldsymbol{r})\cdot\int_\Gamma ds'\ \frac{\boldsymbol{f}_n(\boldsymbol{r}')}{4\pi R} \qquad (59)\\
&= \left[\mathbf{Z}_{\text{stat}}^s\right]_{mn}. \qquad (60)
\end{aligned}$$

The star-loop part (40b) and loop-star part (40c) are, up to a factor Δt, equal to $\mathbf{Z}_0^s$ (52):

$$\left[\mathbf{Z}_0'^{LS}\right]_{mn} = \left[\mathbf{Z}_0'^{SL}\right]_{mn} = \frac{1}{\Delta t}\left[\mathbf{Z}_0^s\right]_{mn} = \frac{1}{\Delta t}\left[\mathbf{Z}_{\text{stat}}^s\right]_{mn}. \qquad (61)$$

Finally, the star-star part is split in two contributions

$$\begin{aligned}
\left[\mathbf{Z}_0'^{SS}\right]_{mn} &= \left[\mathbf{Z}_{s,0}'^{SS}\right]_{mn}+\left[\mathbf{Z}_{h,0}'^{SS}\right]_{mn}, \qquad (62)\\
\left[\mathbf{Z}_{h,0}'^{SS}\right]_{mn} &= \eta\int_\Gamma ds\ \ (\hat{\boldsymbol{n}}\times\boldsymbol{f}_m(\boldsymbol{r}))\cdot\partial_t\mathcal{T}_h\left\{\boldsymbol{f}_n T_{ph}\right\}(\boldsymbol{r},0),\\
\left[\mathbf{Z}_{s,0}'^{SS}\right]_{mn} &= \eta\int_\Gamma ds\ \ (\hat{\boldsymbol{n}}\times\boldsymbol{f}_m(\boldsymbol{r}))\cdot\partial_t\mathcal{T}_s\left\{\boldsymbol{f}_n T_{ph}\right\}(\boldsymbol{r},0),
\end{aligned}$$

The time dependence of these integrands can be approximated as follows, for $R/c \ll \Delta t$:

$$\begin{aligned}
T_{ph}(0-R/c) &= \frac{1}{2}+\mathcal{O}\left(\frac{R}{c\Delta t}\right), \qquad (63)\\
\partial_t^2 T_{ph}(0-R/c) &= \frac{1}{\Delta t^2}. \qquad (64)
\end{aligned}$$

Then,

$$\begin{aligned}
\left[\mathbf{Z}_{s,0}'^{SS}\right]_{mn} &= \frac{1}{\Delta t^2}\left[\mathbf{Z}_{\text{stat}}^s\right]_{mn}, \qquad (65)\\
\left[\mathbf{Z}_{h,0}'^{SS}\right]_{mn} &= -\epsilon\int_\Gamma ds\ \nabla\cdot\boldsymbol{f}_m(\boldsymbol{r})\\
&\qquad\int_\Gamma ds'\ \frac{\nabla'\cdot\boldsymbol{f}_n(\boldsymbol{r}')}{4\pi R}\left(\frac{1}{2}+\mathcal{O}\left(\frac{R}{c\ \Delta t}\right)\right)\\
&= \frac{1}{2}\left[\mathbf{Z}_{\text{stat}}^h\right]_{mn}+\mathcal{O}(\Delta t^{-1}). \qquad (66)
\end{aligned}$$

Thus, when $\Delta t \to +\infty$,

$$\mathbf{Z}'_0 \to \mathbf{P}^{\Lambda H}\mathbf{Z}^s_{\text{stat}}\mathbf{P}^{\Lambda H} + \frac{1}{2}\mathbf{P}^{\Sigma}\mathbf{Z}^h_{\text{stat}}\mathbf{P}^{\Sigma} + \mathcal{O}\left(\Delta t^{-1}\right), \quad (67)$$

or

$$\mathbf{Z}'_0 \to \begin{pmatrix}\mathbf{P}^{\Lambda H} & \mathbf{P}^{\Sigma}\end{pmatrix}\begin{pmatrix}\mathcal{O}(1) & \mathcal{O}\left(\Delta t^{-1}\right)\\ \mathcal{O}\left(\Delta t^{-1}\right) & \mathcal{O}(1)\end{pmatrix}\begin{pmatrix}\mathbf{P}^{\Lambda H}\\ \mathbf{P}^{\Sigma}\end{pmatrix}, \quad (68)$$

which leads to a condition number that is asymptotically constant. This is the result of rescaling the temporal basis and testing functions associated with the star part with a factor $\frac{1}{\Delta t}$ (equations (35) and (36), respectively). This contrasts with the approach used in [21], where the spatial basis and testing functions were rescaled.

V. Numerical Results

A. Torus

As a first example, scattering by a torus with large radius $0.8\ m$ and small radius $0.2\ m$ (Fig. 3) is examined. The torus is illuminated by a Gaussian-in-time plane wave

$$\boldsymbol{e}^i(\boldsymbol{r},t) = \frac{4A}{w\sqrt{\pi}}\hat{\boldsymbol{p}}\exp\left(-\left(\frac{4}{w}\left(c(t-t_0)-\hat{\boldsymbol{k}}\cdot\boldsymbol{r}\right)\right)^2\right), \quad (69)$$

with amplitude $A = 1\ V$, polarization $\hat{\boldsymbol{p}} = \hat{\mathbf{1}}_x$, direction $\hat{\boldsymbol{k}} = \hat{\mathbf{1}}_z$, width $w = 10\ m$ and time of arrival $t_0 = 100\ ns$.

The torus is approximated by a triangle mesh on which $N_S = 918$ RWG functions are defined. The time step is chosen as $0.83\ ns$ (or $c\Delta t = 0.25\ m$). The scattering problem is solved using the EFIE (Section II), the dot-trick Calderón preconditioned EFIE [16] and the qHP-TDEFIE (Section III).

The resulting current on the edge indicated by the arrow in Fig. 3, is shown in Fig. 4 for the three simulations. At early times ($ct < 75\ m$), the three simulations match very well. However, the EFIE simulation ends in a constant loop current, whereas the dot-trick EFIE simulation exhibits a linearly increasing loop current. With the qHP-TDEFIE, the current expansion coefficient goes down to 10^{-14}, at which point the machine precision comes into play. It has been verified that the resulting current is not a static loop current but random numerical noise.

Next, the time step is increased in order to study the low frequency limit of the matrix $\mathbf{Z}_0$. Its condition number is shown in Fig. 5 for the EFIE, the dot-trick EFIE and the qHP-TDEFIE. Whereas for the EFIE and the dot-trick EFIE, the condition number grows proportional to Δt^2, the qHP-TDEFIE remains constant.

B. Static Nullspace

Consider an MOT system with a finite number N_X of nonzero interaction matrices

$$-\mathbf{X}_0\mathsf{j}_i = \sum_{j=1}^{N_X}\mathbf{X}_j\mathsf{j}_{i-j} + \mathsf{e}_i. \quad (70)$$

The convolution operator allows constant-in-time regime solutions if

$$\exists \mathsf{j}_c : \sum_{i=0}^{N_X}\mathbf{X}_i\mathsf{j}_c = 0, \quad (71)$$

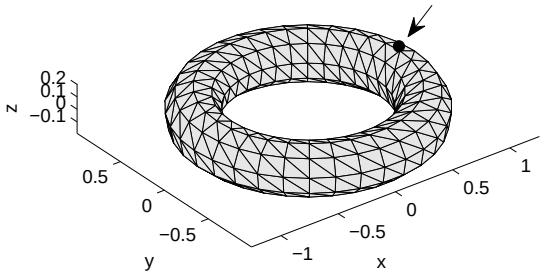

Fig. 3. Triangle mesh for a torus. The arrow points toward the edge on which the current is observed in Fig. 4.

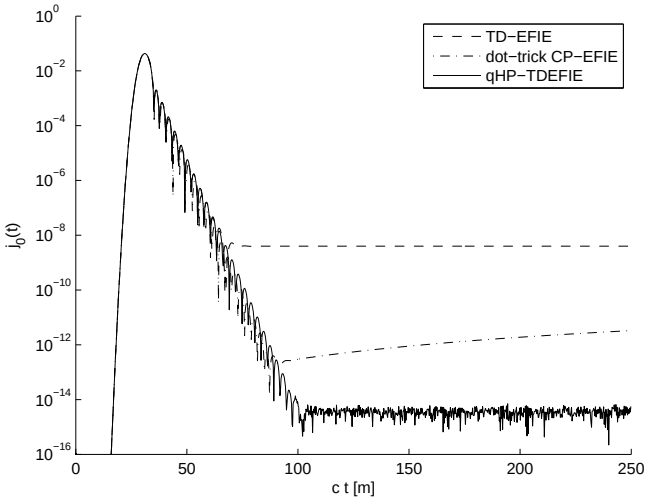

Fig. 4. Current on the torus, obtained using three different formulations. The standard TD-EFIE exhibits a constant-in-time DC instablity. The dot-trick Calderón preconditioned EFIE suffers from a linear-in-time DC instability. The qHP-TDEFIE is immune to DC instability.

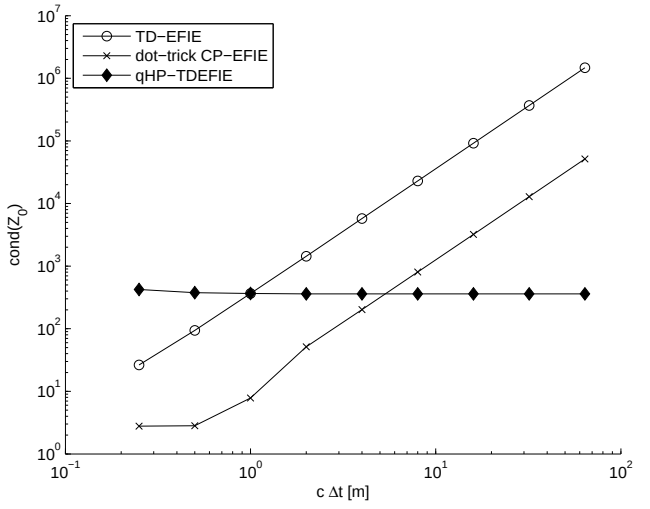

Fig. 5. $\text{cond}(\mathbf{Z}_0)$ for the torus, as a function of the time step Δt.

and linear-in-time regime solutions if

$$\exists \mathsf{j}_l : \sum_{i=0}^{N_X} \mathbf{X}_i (N_X - i + 1) \mathsf{j}_l = 0. \tag{72}$$

In other words, the constant and linear nullspaces of the operator $\mathbf{X}_i$ can be investigated by computing the spectrum of

$$\mathbf{X}_c = \sum_{i=0}^{N_X} \mathbf{X}_i, \tag{73}$$

$$\mathbf{X}_l = \sum_{i=0}^{N_X} (N_X - i + 1) \mathbf{X}_i. \tag{74}$$

This approach can readily be applied to the dot-trick EFIE and the qHP-TDEFIE. For the standard EFIE, there are an unlimited number of nonzero interaction matrices. This is only a technical complication, which is resolved in Appendix B. This type of analysis is much cheaper than a full eigenvalue analysis on the system's companion matrix (see [16]).

1) Cuboid: Now consider the cuboid mesh with dimensions $2 \times 2 \times 2/3 \ m$ in Fig. 6. On this mesh, $N_S = 360$ RWG functions are defined, which can be combined into 121 independent loops. The time step is fixed at $c\Delta t = 1 \ m$.

The singular values of $\mathbf{X}_c$ are shown in Fig. 7, top, for the standard TD-EFIE, the dot-trick CP-EFIE and the qHP-TDEFIE. The 121 singular values smaller than 10^{-14} correspond to the constant loop currents that reside in the nullspace of the EFIE operator. The dot-trick CP-EFIE and the qHP-TDEFIE do not exhibit a constant-in-time nullspace.

The singular values of $\mathbf{X}_l$ are shown in Fig. 7, bottom. The absence of very small singular values indicates that none of the three formulations exhibit a linear-in-time nullspace.

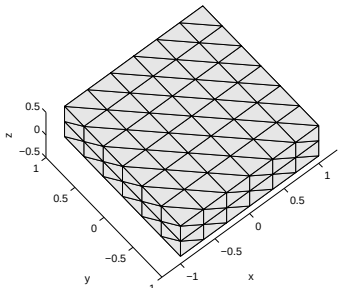

Fig. 6. Cuboid ($2 \times 2 \times 2/3$ m) mesh, $N_S = 360$.

2) Rectangular Torus: The experiment is now repeated for the rectangular torus shown in Fig. 8. On this mesh, 384 RWG functions are defined, which can be combined into 127 local and 2 global loops.

Fig. 9 shows that the constant-in-time loops (127 local loops, and 2 global loops) are again in the nullspace of the EFIE. The nullspace of the dot-trick EFIE encompasses both constant-in-time and linear-in-time global loops. The qHP-TDEFIE again does not exhibit a static nullspace.

VI. Conclusion

The quasi-Helmholtz Projected TD-EFIE developed in this contribution, is a novel formulation of the TD-EFIE that is immune to spurious static currents, on both simply and multiply connected structures. While it is based on the separation of quasi-Helmholtz components, it does not require the explicit construction of a loop-star or a loop-tree basis, nor the detection of global loops. The qHP-TDEFIE is discretized in time using a Galerkin method, with different basis and testing function combinations for each component. This is necessary in order to obtain a stable marching-on-in-time scheme. The temporal basis and testing functions are chosen such that the resulting system of equations is immune to low frequency breakdown, i.e., the system remains well conditioned for large time steps.

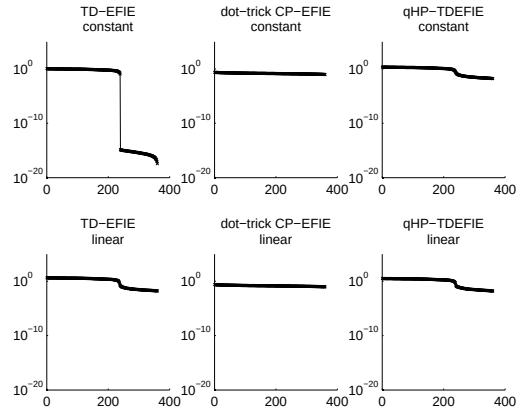

Fig. 7. Spectral analysis of the static nullspace of the cuboid. Top: constant-in-time currents, bottom: linear-in-time currents.

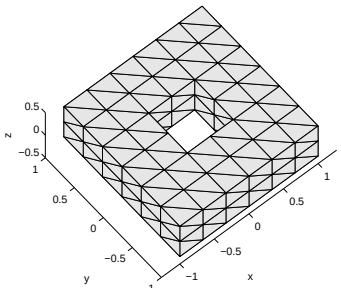

Fig. 8. Rectangular torus mesh, $N_S = 384$.

Appendix

A. Alternative Form

1) Standard EFIE: In Section II, a temporal Galerkin discretization of the TD-EFIE was proposed, in which the temporal testing and trial functions are both pulses $p(t - i\Delta t)$. This yields a current that is piecewise constant in time. Alternatively, it is also possible to expand the current in hat functions:

$$\mathsf{j}(t) = \sum_{i=1}^{N_T} \mathsf{j}_i \ h(t - i\Delta t). \tag{75}$$

A stable MOT scheme can be obtained by testing the TD-EFIE with Dirac distributions:

$$\int_{\mathbb{R}} \delta(t - j\Delta t) \, (\text{Eq. (9)}) \, dt \qquad j = 1, 2, 3, ..., N_T. \tag{76}$$

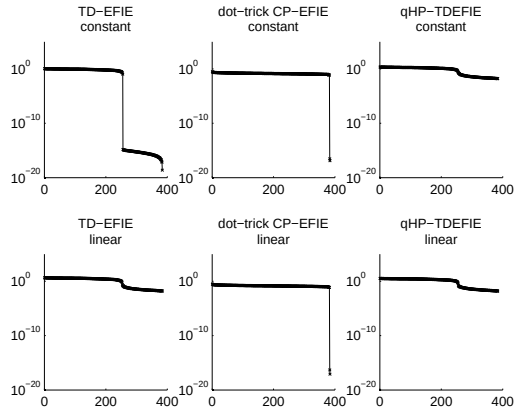

Fig. 9. Spectral analysis of the static nullspace of the rectangular torus. Top: constant-in-time currents, bottom: linear-in-time currents.

Since

$$\begin{aligned} & \eta \int_{\mathbb{R}} dt\ \delta(t-i\Delta t) \int_{\Gamma} (\hat{\boldsymbol{n}} \times \boldsymbol{f}_m(\boldsymbol{r})) \cdot \mathcal{T}\left\{\boldsymbol{f}_n h\right\}(\boldsymbol{r},t) ds \\ = & \frac{\eta}{\Delta t} \int_{\mathbb{R}} dt\ p(t-i\Delta t) \int_{\Gamma} (\hat{\boldsymbol{n}} \times \boldsymbol{f}_m(\boldsymbol{r})) \cdot \mathcal{T}\left\{\boldsymbol{f}_n p\right\}(\boldsymbol{r},t) ds \\ = & \frac{1}{\Delta t} \mathbf{Z}_i, \end{aligned} \tag{77}$$

the interaction matrices and therefore the properties concerning stability and nullspaces are identical.

2) qHP-TDEFIE: A qHP-TDEFIE similar to this scheme can be developed by defining the auxiliary unknown $y(t)$ as

$$\begin{aligned} & \mathsf{y}(t) = \left(\mathbf{P}^{\Sigma} + \partial_t \mathbf{P}^{\Lambda H}\right) \mathsf{j}(t) \\ \Longleftrightarrow \quad & \mathsf{j}(t) = \left(\mathbf{P}^{\Sigma} + \partial_t^{-1} \mathbf{P}^{\Lambda H}\right) \mathsf{y}(t), \end{aligned} \tag{78}$$

satisfying

$$\mathcal{Z}' \mathsf{y}(t) = -\left(\mathbf{P}^{\Lambda H} + \partial_t \mathbf{P}^{\Sigma}\right) \mathsf{e}(t). \tag{79}$$

The operator $\mathcal{Z}'$ is the same as in Section III-B, since

$$\begin{aligned} \mathcal{Z}' &= \left(\partial_t^{-1} \mathbf{P}^{\Lambda H} + \mathbf{P}^{\Sigma}\right) \mathcal{Z} \left(\mathbf{P}^{\Lambda H} + \partial_t \mathbf{P}^{\Sigma}\right) \\ &= \left(\mathbf{P}^{\Lambda H} + \partial_t \mathbf{P}^{\Sigma}\right) \mathcal{Z} \left(\partial_t^{-1} \mathbf{P}^{\Lambda H} + \mathbf{P}^{\Sigma}\right). \end{aligned} \tag{80}$$

The temporal discretization of (79) is the similar as in Section III-C, with only minor modifications:

$$\mathsf{e'}_j = \int_{\mathbb{R}} \left(\delta(t-j\Delta t)\mathbf{P}^{\Lambda H} + \frac{1}{\Delta t} p(t-j\Delta t)\partial_t \mathbf{P}^{\Sigma}\right) \mathsf{e}(t)\ dt, \tag{81}$$

$$\boldsymbol{j}(\boldsymbol{r},t) = \sum_{m=1}^{N_S} \sum_{j=1}^{N_T} \left[\mathbf{P}^{\Sigma} \mathsf{y}_j + \Delta t \sum_{i=1}^{j} \mathbf{P}^{\Lambda H} \mathsf{y}_i\right]_m h(t-j\Delta t) \boldsymbol{f}_m(\boldsymbol{r}). \tag{82}$$

This results in a current that is also expanded in hats instead of pulses. The MOT matrices $\mathbf{Z}'_i$ are the same as in Section III. Therefore, this alternative scheme is also stable, and free of a static nullspace. Even though the numerical integration of $\mathbf{P}^{\Lambda H}\mathsf{y}(t)$ ($\Delta t \sum_{i=1}^{j} \mathbf{P}^{\Lambda H}\mathsf{y}_i$ in (82)) can result in a nonzero loop component in $\mathsf{j}(t)$, it can never lead to DC instabilities.

B. Spectral Analysis of the Static Null Space for the EFIE

The hypersingular EFIO $\mathcal{T}_h$ contains a temporal integral, which corresponds to the integration of the current in order to obtain the electrical charge on Γ. This integral is transformed into an infinite summation by the discretization procedure, i.e., an infinite number of matrices $\mathbf{Z}_i \neq 0$.

It is therefore convenient to introduce additional unknowns to discretize the temporal integral of $\mathsf{j}(t)$

$$\mathsf{s}(t) = \partial_t^{-1} \mathsf{j}(t) = \sum_{i=1}^{N_T} \mathsf{s}_i\ h(t-i\Delta t), \tag{83}$$

$$\mathsf{s}_i = \Delta t \sum_{j=0}^{i} \mathsf{j}_i. \tag{84}$$

Then,

$$\sum_{i=0}^{j} \mathbf{Z}_i \mathsf{j}_{j-i} = \sum_{i=0}^{j} \mathbf{Z}^s_i \mathsf{j}_{j-i} + \sum_{i=0}^{j} \dot{\mathbf{Z}}^h_i \mathsf{s}_{j-i}, \tag{85}$$

$$\begin{aligned} \left[\mathbf{Z}^s_i\right]_{mn} &= \eta \int_{\mathbb{R}} dt\ p(t-i\Delta t) \\ & \qquad \int_{\Gamma} (\hat{\boldsymbol{n}} \times \boldsymbol{f}_m(\boldsymbol{r})) \cdot \mathcal{T}_s\left\{\boldsymbol{f}_n p\right\}(\boldsymbol{r},t) ds, \end{aligned} \tag{86}$$

$$\begin{aligned} \left[\dot{\mathbf{Z}}^h_i\right]_{mn} &= \eta \int_{\mathbb{R}} dt\ p(t-i\Delta t) \\ & \qquad \int_{\Gamma} (\hat{\boldsymbol{n}} \times \boldsymbol{f}_m(\boldsymbol{r})) \cdot \partial_t \mathcal{T}_h\left\{\boldsymbol{f}_n h\right\}(\boldsymbol{r},t) ds \end{aligned} \tag{87}$$

where $\mathbf{Z}^s_i = \dot{\mathbf{Z}}^h_i = 0$ for $i > N_Z$. Currents that are constant in time satisfy

$$\mathsf{j}_i = \mathsf{j}_c, \tag{88}$$

$$\mathsf{s}_i = (i+1)\Delta t\ \mathsf{j}_c, \tag{89}$$

and belong to the null space of the EFIE if

$$\left(\sum_i \mathbf{Z}^s_i + \Delta t \sum_i (N_Z - i + 1)\dot{\mathbf{Z}}^h_i\right) \mathsf{j}_c = 0. \tag{90}$$

Currents that are linear in time satisfy

$$\mathsf{j}_i = (i+1)\mathsf{j}_l, \tag{91}$$

$$\mathsf{s}_i = \Delta t \frac{(i+1)(i+2)}{2} \mathsf{j}_l, \tag{92}$$

and belong to the null space of the EFIE if

$$\begin{aligned} & \left(\sum_i (N_Z - i + 1)\mathbf{Z}^s_i\right) \mathsf{j}_l \\ + & \Delta t \left(\sum_i \frac{(N_Z - i + 1)(N_Z - i + 2)}{2} \dot{\mathbf{Z}}^h_i\right) \mathsf{j}_l = 0 \end{aligned} \tag{93}$$

Therefore, the static null space of the EFIE operator can be investigated by computing the spectrum of

$$\mathbf{X}_c = \sum_i \mathbf{Z}^s_i + \Delta t \sum_i (N_Z - i + 1)\dot{\mathbf{Z}}^h_i, \tag{94}$$

$$\begin{aligned} \mathbf{X}_l = & \sum_i (N_Z - i + 1)\mathbf{Z}^s_i \\ & + \Delta t \sum_i \frac{(N_Z - i + 1)(N_Z - i + 2)}{2} \dot{\mathbf{Z}}^h_i. \end{aligned} \tag{95}$$

ACKNOWLEDGMENT

The work of Y. Beghein was supported by a doctoral grant from the Agency for Innovation by Science and Technology in Flanders (IWT).

REFERENCES

[1] C. L. Bennett and W. L. Weeks, "A technique for computing approximate electromagnetic impulse response of conducting bodies," Ph.D. dissertation, Purdue University., 1968.

[2] S. M. Rao and D. R. Wilton, "Transient scattering by conducting surfaces of arbitrary shape," *Antennas and Propagation, IEEE Transactions on*, vol. 39, no. 1, pp. 56–61, 1991.

[3] Y.-s. Chung, T. K. Sarkar, and B. H. Jung, "Solution of a time-domain magnetic-field integral equation for arbitrarily closed conducting bodies using an unconditionally stable methodology," *Microwave and Optical Technology Letters*, vol. 35, no. 6, pp. 493–499, 2002.

[4] M.-D. Zhu, X.-L. Zhou, and W.-Y. Yin, "Efficient evaluation of double surface integrals in time-domain integral equation formulations," *Antennas and Propagation, IEEE Transactions on*, vol. 61, no. 9, pp. 4653–4664, Sept 2013.

[5] B. Shanker, M. Lu, J. Yuan, and E. Michielssen, "Time domain integral equation analysis of scattering from composite bodies via exact evaluation of radiation fields," *Antennas and Propagation, IEEE Transactions on*, vol. 57, no. 5, pp. 1506–1520, May 2009.

[6] A. Yucel and A. Ergin, "Exact evaluation of retarded-time potential integrals for the RWG bases," *Antennas and Propagation, IEEE Transactions on*, vol. 54, no. 5, pp. 1496–1502, May 2006.

[7] Y. Shi, M.-Y. Xia, R. shan Chen, E. Michielssen, and M. Lu, "Stable electric field TDIE solvers via quasi-exact evaluation of MOT matrix elements," *Antennas and Propagation, IEEE Transactions on*, vol. 59, no. 2, pp. 574–585, Feb 2011.

[8] A. Geranmayeh, W. Ackermann, and T. Weiland, "Temporal discretization choices for stable boundary element methods in electromagnetic scattering problems," *Applied Numerical Mathematics*, vol. 59, no. 11, pp. 2751 – 2773, 2009, special Issue: Boundary Elements Theory and Applications, {BETA} 2007 Dedicated to Professor Ernst P. Stephan on the Occasion of his 60th Birthday.

[9] E. van 't Wout, D. Van der Heul, H. van der Ven, and C. Vuik, "Design of temporal basis functions for time domain integral equation methods with predefined accuracy and smoothness," *Antennas and Propagation, IEEE Transactions on*, vol. 61, no. 1, pp. 271–280, Jan 2013.

[10] Y. Beghein, K. Cools, H. Bagci, and D. De Zutter, "A space-time mixed galerkin marching-on-in-time scheme for the time-domain combined field integral equation," *Antennas and Propagation, IEEE Transactions on*, vol. 61, no. 3, pp. 1228–1238, March 2013.

[11] Y. Beghein, K. Cools, and D. De Zutter, "A temporal Galerkin discretization of the charge-current continuity equation," in *2013 International Conference on Electromagnetics in Advanced Applications (ICEAA)*, Sept 2013, pp. 628–631.

[12] I. Terrasse, "Résolution mathématique et numérique des équations de maxwell instationnaires par une méthode de potentiels retardés," Ph.D. dissertation, 1993.

[13] A. Pray, Y. Beghein, N. Nair, K. Cools, H. Bagci, and B. Shanker, "A higher order space-time galerkin scheme for time domain integral equations," *Antennas and Propagation, IEEE Transactions on*, vol. 62, no. 12, pp. 6183–6191, Dec 2014.

[14] F. Valdes, M. Ghaffari-Miab, F. Andriulli, K. Cools, J. Kotulski, and E. Michielssen, "High-order calderón multiplicative preconditioner for time domain electric field integral equations," in *Antennas and Propagation (APSURSI), 2011 IEEE International Symposium on*, July 2011, pp. 2362–2362.

[15] Y. Shi, H. Bagci, and M. Lu, "On the internal resonant modes in marching-on-in-time solution of the time domain electric field integral equation," *Antennas and Propagation, IEEE Transactions on*, vol. 61, no. 8, pp. 4389–4392, Aug 2013.

[16] F. Andriulli, K. Cools, F. Olyslager, and E. Michielssen, "Time domain calderón identities and their application to the integral equation analysis of scattering by PEC objects part II: Stability," *Antennas and Propagation, IEEE Transactions on*, vol. 57, no. 8, pp. 2365–2375, Aug 2009.

[17] Y. Shi, H. Bagci, and M. Lu, "On the static loop modes in the marching-on-in-time solution of the time-domain electric field integral equation," *Antennas and Wireless Propagation Letters, IEEE*, vol. 13, pp. 317–320, 2014.

[18] K. Cools, F. Andriulli, F. Olyslager, and E. Michielssen, "Time domain calderón identities and their application to the integral equation analysis of scattering by PEC objects part I: Preconditioning," *Antennas and Propagation, IEEE Transactions on*, vol. 57, no. 8, pp. 2352–2364, Aug 2009.

[19] ——, "Nullspaces of MFIE and Calderón preconditioned efie operators applied to toroidal surfaces," *Antennas and Propagation, IEEE Transactions on*, vol. 57, no. 10, pp. 3205–3215, Oct 2009.

[20] F. Andriulli, H. Bagci, F. Vipiana, G. Vecchi, and E. Michielssen, "Analysis and regularization of the td-efie low-frequency breakdown," *Antennas and Propagation, IEEE Transactions on*, vol. 57, no. 7, pp. 2034–2046, July 2009.

[21] N.-W. Chen, K. Aygun, and E. Michielssen, "Integral-equation-based analysis of transient scattering and radiation from conducting bodies at very low frequencies," *Microwaves, Antennas and Propagation, IEE Proceedings*, vol. 148, no. 6, pp. 381–387, Dec 2001.

[22] F. Andriulli, K. Cools, I. Bogaert, and E. Michielssen, "On a well-conditioned electric field integral operator for multiply connected geometries," *Antennas and Propagation, IEEE Transactions on*, vol. 61, no. 4, pp. 2077–2087, April 2013.

[23] I. Bogaert, K. Cools, F. P. Andriulli, and H. Bagci, "Low-frequency scaling of the standard and mixed magnetic field and müller integral equations," *Antennas and Propagation, IEEE Transactions on*, vol. 62, no. 2, pp. 822–831, 2014.

[24] F. Andriulli, "Loop-star and loop-tree decompositions: Analysis and efficient algorithms," *Antennas and Propagation, IEEE Transactions on*, vol. 60, no. 5, pp. 2347–2356, May 2012.

[25] G. Pisharody and D. S. Weile, "Robust solution of time-domain integral equations using loop-tree decomposition and bandlimited extrapolation," *Antennas and Propagation, IEEE Transactions on*, vol. 53, no. 6, pp. 2089–2098, June 2005.

[26] D. S. Weile, G. Pisharody, N.-W. Chen, B. Shanker, and E. Michielssen, "A novel scheme for the solution of the time-domain integral equations of electromagnetics," *Antennas and Propagation, IEEE Transactions on*, vol. 52, no. 1, pp. 283–295, Jan 2004.

[27] K. Aygun, B. Shanker, A. A. Ergin, and E. Michielssen, "A two-level plane wave time-domain algorithm for fast analysis of emc/emi problems," *Electromagnetic Compatibility, IEEE Transactions on*, vol. 44, no. 1, pp. 152–164, 2002.

[28] A. A. Ergin, B. Shanker, and E. Michielssen, "The plane-wave time-domain algorithm for the fast analysis of transient wave phenomena," *Antennas and Propagation Magazine, IEEE*, vol. 41, no. 4, pp. 39–52, 1999.

[29] S. Rao, D. Wilton, and A. Glisson, "Electromagnetic scattering by surfaces of arbitrary shape," *IEEE Trans. Antennas Propag.,*, vol. 30, no. 3, pp. 409 – 418, may 1982.

[30] A. Pray, N. Nair, and B. Shanker, "Stability properties of the time domain electric field integral equation using a separable approximation for the convolution with the retarded potential," *Antennas and Propagation, IEEE Transactions on*, vol. 60, no. 8, pp. 3772–3781, Aug 2012.

[31] F. P. Andriulli, "Loop-star and loop-tree decompositions: Analysis and efficient algorithms," *Antennas and Propagation, IEEE Transactions on*, vol. 60, no. 5, pp. 2347–2356, 2012.

Yves Beghein received the M.Sc.Eng. degree in Engineering Physics from Ghent University, Belgium, in 2011. His master's dissertation dealt with the efficient modeling of scattering by chiral media. He is currently pursuing a Ph.D. degree at the Electromagnetics Group at Ghent University, under the advisorship of Prof. Kristof Cools (University of Nottingham, U.K.) and Prof. Daniël De Zutter (Ghent University). His research focusses on both time domain and frequency domain boundary element methods, their stable and accurate discretizations, and efficient solution methods.

Kristof Cools received the MEng degree in Applied Physics Engineering from Ghent University, Belgium, in 2004. His master's dissertation dealt with the full wave simulation of metamaterials using the low frequency multilevel fast multipole method. He received the Ph.D. degree from Ghent University in 2008, under the advisership of Prof. F. Olyslager and Prof. Eric Michielssen. In 2008, he was awarded the Young Scientist Best Paper award at the International Conference on Electromagnetics and Advanced Applications. In 2011, he was a visiting research fellow at TELECOM Bretagne. In November 2011, he took up a position as Lecturer in Computational Electromagnetics at the University of Nottingham. His current focuses on the spectral properties of the boundary integral operators of electromagnetics, on stable and accurate discretization schemes for frequency and time domain boundary element methods, on domain decomposition techniques, and on the implementations of algorithms from computational physics for high performance computing.

Francesco P. Andriulli Francesco P. Andriulli (S 05, M 09, SM 11) received the Laurea in electrical engineering from the Politecnico di Torino, Italy, in 2004, the MSc in electrical engineering and computer science from the University of Illinois at Chicago in 2004, and the PhD in electrical engineering from the University of Michigan at Ann Arbor in 2008. From 2008 to 2010 he was a Research Associate with the Politecnico di Torino. Since 2010 he has been with the École nationale supérieure des télécommunications de Bretagne (TELECOM Bretagne), Brest, France, where he is currently a Full Professor. His research interests are in computational electromagnetics with focus on frequency- and time-domain integral equation solvers, well-conditioned formulations, fast solvers, low-frequency electromagnetic analysis, and simulation techniques for antennas, wireless components, microwave circuits, and biomedical applications.

Dr. Andriulli was the recipient of the best student paper award at the 2007 URSI North American Radio Science Meeting. He received the first place prize of the student paper context of the 2008 IEEE Antennas and Propagation Society International Symposium. He was the recipient of the 2009 RMTG Award for junior researchers and was awarded two URSI Young Scientist Awards at the International Symposium on Electromagnetic Theory in 2010 and 2013 where he was also awarded the second prize in the best paper contest. In addition, he co-authored another first prize conference paper (ICEAA 2009), two honourable mention conference papers (ICEAA 2011, URSI/IEEE-APS 2013), and other three finalist conference papers (URSI/IEEE-APS 2012, URSI/IEEE-APS 2007, URSI/IEEE-APS 2006). Moreover, he received the 2014 IEEE AP-S Donald G. Dudley Jr. Undergraduate Teaching Award, the 2014 URSI Issac Koga Gold Medal and the 2015 EurAAP Leopold B. Felsen Award for Excellence in Electrodynamics.

Dr. Andriulli is a member of Eta Kappa Nu, Tau Beta Pi, Phi Kappa Phi, and of the International Union of Radio Science (URSI). He serves as an Associate Editor for the *IEEE Transactions on Antennas and Propagation*, *IEEE Antennas and Wireless Propagation Letters*, and *IEEE Access*.